Design and Test of Pipeline Leak Detector With Acoustic Resonance Air Cavity

Huang Xinjing, Ren Xiaoyu, Wang Liang, Bian Xu, Li Jian, and Ma Jinyu

***Abstract*—Early detection of continuous small leaks in pipeline infrastructure is crucial for preventing major failures, yet existing methods often struggle with sensitivity limitations and practical deployment challenges. This article presents an innovative approach using a spherical detector (SD) with an acoustic resonant air cavity (ARAC), which addresses these challenges by combining the advantages of free-swimming mobility with enhanced acoustic sensitivity. The ARAC design leverages acoustic resonance principles to amplify leak-induced sounds, while the SD's mobility allows direct access to leak locations within pipelines. Through systematic investigation of cavity dimensions and resonance modes via finite element analysis, we establish the relationship between ARAC size and detection sensitivity. Laboratory experiments with multiple SD prototypes demonstrate that larger cavities (>96 mm diameter) achieve superior sensitivity by effectively capturing low-frequency (100–5000 Hz) leak signals through their first three resonance modes. A signal processing algorithm combining wavelet decomposition and adaptive thresholding is developed to distinguish leak signals from mechanical impacts, achieving detection rates exceeding 95% for leaks 0.6–1.0 mm in diameter. Field validation tests with an optimized aluminum SD prototype confirm the reliable detection of 1 mm leaks under both high (1 MPa) and low (0.5 MPa) pressure conditions while rolling through operational pipelines. Quantitative analysis reveals that the system maintains effective detection capability even under challenging field conditions, with the algorithm successfully filtering out interference from pipe wall collisions and environmental noise. These findings demonstrate the practical viability of ARAC-based detection technology for pipeline infrastructure monitoring and maintenance.**

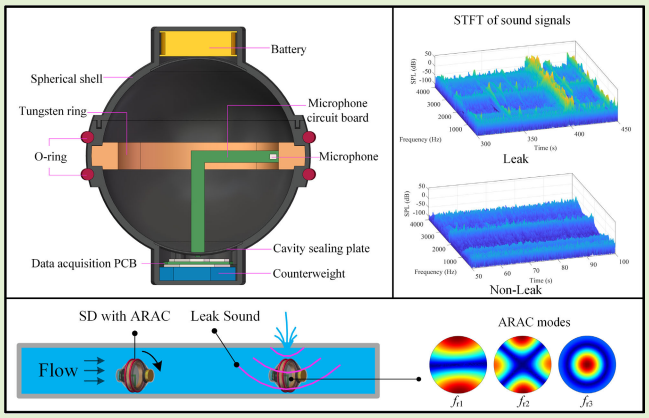

***Index Terms*— Leak detection, pipeline, resonant cavity, spherical detector (SD).**

I. Introduction

PIPELINE leaks can lead to severe consequences, including environmental damage and economic losses. In the case of oil pipelines, leaks can result in substantial oil seepage into soil and water, causing ecosystem destruction and economic repercussions [1], [2]. In water supply pipelines, leaks can lead to water resource wastage and contamination of drinking water [3]. Notably, significant leaks, such as sudden pipe bursts, often stem from continuous small leaks that are challenging to detect promptly. Early detection of continuous small leaks is particularly challenging due to their subtle nature, yet these minor leaks often precede catastrophic pipeline failures. Effective detection methods for small leaks are, therefore, crucial for preventing major accidents and environmental damage. The timely identification and repair of pipeline leaks, particularly continuous minor leaks in their early stages, are, therefore, imperative to ensure the safe operation of pipelines.

In spite of the critical role of traditional leak detection methods, they exhibit inherent limitations that can impede their effectiveness. The Mass-Volume Balance methods [4] operate based on monitoring and comparing the expected and actual mass or volume of fluid passing through a section of a pipeline. They offer advantages, such as simplicity in setup, and the ability to detect anomalies by highlighting discrepancies in mass or volume balance. They, however, cannot localize the leak point, and their accuracy can be significantly affected

Received 15 November 2024; accepted 15 December 2024. Date of publication 25 December 2024; date of current version 31 January 2025. This work was supported in part by the National Natural Science Foundation of China under Grant 62073233 and Grant 62473279 and in part by the Guangxi Key Laboratory of Automatic Detecting Technology and Instruments Foundation under Grant YQ24203. The associate editor coordinating the review of this article and approving it for publication was Dr. Wei Wei. *(Corresponding author: Ma Jinyu.)*

Huang Xinjing, Ren Xiaoyu, Wang Liang, Li Jian, and Ma Jinyu are with the State Key Laboratory of Precision Measurement Technology and Instruments, Tianjin University, Tianjin 300072, China (e-mail: huangxinjing@tju.edu.cn; jinyu.ma@tju.edu.cn).

Bian Xu is with the State Key Laboratory of Precision Measurement Technology and Instruments, Tianjin University, Tianjin 300072, China, and also with Tianjin Renai College, Tianjin 300072, China.

Digital Object Identifier 10.1109/JSEN.2024.3520131

by normal fluctuations in flow rates associated with transport tasks or rapidly changing operation conditions, which may lead to false positives or missed detections. Negative pressure wave (NPW) methods [5], [6] detect leaks by using pressure sensors installed at both ends of the pipeline to locate the leak based on the time difference between the propagation of leak caused by NPWs reaching the two ends. NPW method can quickly and accurately identify the location of large and sudden leaks but is ineffective for slow, small, and continuous leaks that do not generate pressure changes. Vibration monitoring methods usually based on accelerometers [7], [8] operate by detecting the vibrational energy produced by a leak along the pipeline walls. While effective in identifying the presence of leaks through changes in vibration patterns, their performance significantly deteriorates over long distances due to signal attenuation, and they necessitate a dense sensor deployment along the pipeline, which can be cost-prohibitive. Similarly, fiber optic sensing (FOS) technology offers a sophisticated approach to leak detection by measuring both vibrational and thermal changes along the pipeline [9]. Using technologies, such as phase-sensitive optical time domain reflectometry (Φ-OTDR) [10], [11] and Brillouin optical time domain reflectometry (B-OTDR) [11], [12], FOS systems can pinpoint the location of a leak by detecting changes in the backscattered light caused by leak induced vibrations and temperature shifts in the surrounding soil. The main drawback of FOS technology is, however, the necessity of embedding optical fibers during the construction phase of the pipeline, which adds to the complexity and cost; particularly, older pipelines do not have such FOS infrastructure. Acoustic methods, employing devices like listening rods [13], leverage the sounds generated by leaks and propagate through air and soil to detect and locate the leaks. These methods are highly intuitive and can be applied without the need for complex setups. They are, however, suitable for further investigations into suspected leaks and cannot cover the whole deeply buried pipelines. They may be impeded by background noise, which often makes it difficult to detect leaks in noisy environments or where the leak sound signal is weak.

In recent years, free-swimming detection methods within pipelines have been developed [14]. These methods rely on robots that move inside pipelines, which are equipped with a variety of sensors. They do not require external connection cables and only rely on the liquid flow in the pipeline to propel them. They can approach any point in the whole pipeline, so they excel in detecting leak sounds near the leak point within the pipeline, providing exceptional leak detection sensitivity and high accuracy. Pipeline inspection gauges (PIGs) [14], [15], [16] move along the pipeline driven by the pressure difference between front and rear. Because of their bowl shells being close to the pipe walls, they are prone to clogging issues, and the leak sound may be drowned out by the sound of the bowl rubbing against the wall. The MTA Pipe-Inspector,[1] proposed by Henrich et al. [17], is an untethered image acquisition free swimming (FS) system for leak and inner wall defect inspection. It is also equipped with other sensors like Sonar, 3-D Laser, etc. Özaslan et al. [18] proposed an FS system equipped with high acoustic sensitivity to redundantly detect leaks. Based on the phenomenon that a sharp pressure drop will occur in a small region around the leak, Wu et al. [19] developed a force-sensing-based leak sensor, which resembles a small PIG. Spherical detectors (SDs) [14], smaller in diameter than the pipe, roll forward propelled by the pipeline fluid and can offer easy deployment and retrieval with lower risk of clogging and reduced costs. These intelligent spheres carry acoustic sensors [20], accelerometers, or gyroscopes [21], to record data on movement and environmental sounds while traversing through the whole pipeline. This data is analyzed to pinpoint the location of leaks. An area is considered to have a leak if there is a significant increase in acoustic power in the characteristic spectrum [7], [22].

Early research efforts about SDs [22], [23], [24] focused on how to seal various sensors and electronic components within a spherical shell and ensure the waterproof capacity and adaptability to high-pressure environments within the pipeline. The SD's shell typically comprises an inner pressure-resistant aluminum shell and a thick outer polyurethane shell, which would significantly attenuate incoming leak sounds and lower the leak detection sensitivity. Previous research on SDs has primarily focused on basic structural design and sensor integration, with limited attention to optimizing acoustic sensitivity. The incorporation of acoustic resonant cavities represents a significant advancement in SD technology, potentially offering enhanced detection capabilities while maintaining the practical advantages of free-swimming operation. In recent years, Tianjin University [25], [26] has redesigned and improved the SD's structure by considering the acoustic sensing principle of the leak-pipe-SD system. They proposed a design that incorporates as many electronic components as possible into the spherical shell to create a large air cavity that generates acoustic resonance to achieve highly sensitive detection of small pipeline leaks [25]. In a static state, an SD with an acoustic resonate air cavity can achieve detection sensitivity as high as 0.164 L/min for small continuous leaks. When an acoustic resonant air cavity (ARAC) is contained in a moving SD, it is necessary to study how to select the size of the ARAC and the acoustic resonance mode to obtain highly sensitive detection of leak sound, and to verify that SD containing ARAC can detect pipeline leaks while rolling rather than being stationary.

This research aims to address these technological gaps by developing and validating an innovative SD design that leverages acoustic resonance principles to enhance leak detection sensitivity. The study systematically investigates the relationship between cavity design parameters and detection performance while also addressing practical implementation challenges in operational pipeline environments. The remainder of this article is organized as follows.

Section II presents the operating principles of the SD and ARAC, detailing the theoretical foundations and analyzing the interactions between the pipeline environment, leak-generated noise signals, and the resonant response through finite element simulations. The analysis of acoustic pressure distribution modes and frequency response characteristics provides the basis for subsequent SD design optimization.

[1]Registered trademark.

Section III focuses on experimental validation through laboratory testing. SD prototypes with different ARAC sizes are designed, manufactured, and systematically evaluated to investigate the relationship between cavity dimensions and detection sensitivity. Statistical analysis of the detection results under various leak conditions quantitatively demonstrates the system's performance capabilities.

Section IV describes the development of an optimized aluminum SD for field applications, incorporating insights gained from the laboratory experiments. The design considerations, including structural stability, component layout, and signal acquisition, are thoroughly discussed.

Section V presents comprehensive field validation tests under real pipeline operating conditions. A systematic signal processing algorithm is developed to distinguish leak signals from mechanical impacts and environmental noise. The experimental results demonstrate the SD's capability to detect small leaks under various pressure conditions while rolling through the pipeline.

Sections VI–VII discuss the technical limitations, practical challenges, and future research directions, followed by conclusions summarizing the key findings and contributions. This systematic investigation provides valuable insights for the development and implementation of ARAC-based leak detection systems in pipeline infrastructure maintenance.

II. Leak Detection Principle

The key innovation of the SD design is the use of an ARAC to detect broad-spectrum leak noises. As illustrated in Fig. 1(a), the SD is rolling at the bottom of the pipeline and is driven forward by the fluid flow inside. The effectiveness of ARAC-based detection stems from the correlation between leak sound characteristics and the ARAC's frequency response properties. Pipeline leaks generate acoustic signals with higher energy concentrated in the lower frequency range, exhibiting a gradually decreasing sound pressure level (SPL) as frequency increases. The ARAC is specifically designed to exploit this characteristic through its three resonance modes (f_{r1}, f_{r2}, and f_{r3}), which provide selective frequency amplification. By aligning these resonance frequencies with the high-energy bands of leak sounds, the ARAC achieves enhanced detection sensitivity. When a leak occurs, broadband noise is generated at the leak point and propagates along the pipeline to both sides. As the SD passes the leak point, it detects the sound of the leak, which assists in pinpointing the occurrence of the leak. Leak noise is characterized as a wide-spectrum signal ranging from 100 to 5000 Hz [25], [27], [28], with higher energy at lower frequencies and diminishing energy at higher frequencies. Under the stimulation of external leak noise, the ARAC within the SD resonates at multiple frequencies, and specifically, the first three resonance frequencies are denoted as f_{r1}, f_{r2}, and f_{r3}. As depicted in Fig. 1(b), the sound pressure distribution at frequencies f_{r1} and f_{r2} is concentrated around the edges of the ARAC, while that of f_{r3} is centered. The sound pressure transmitted from the external water to the air cavity is captured by the microphones sealed within the ARAC. Fig. 1(c) shows that the resonance frequencies decrease as the cavity radius increases,

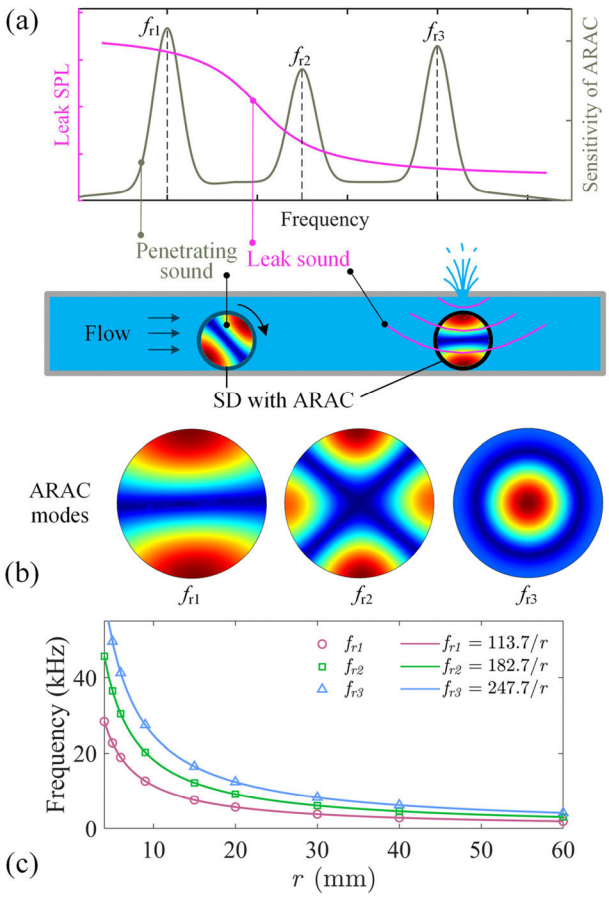

Fig. 1. Principles of SD with a spherical ARAC for liquid-filled pipeline leak detection. (a) Schematic of leak sound SPL and sensitivity of the spherical ARAC. (b) Acoustic pressure distribution modes of ARAC. (c) Relationship between resonant frequency and cavity size [26].

guiding the SD design toward larger resonance cavities to cover the leak noise bandwidth up to 5000 Hz; therefore, The SD design must address two key requirements. First, its resonance frequencies (f_{r1}, f_{r2}, f_{r3}) should fall within the leak noise bandwidth. Second, the microphone location within the resonance cavity must be optimized to maximize detection sensitivity and accuracy.

To analyze the frequency response of the SD to excitation sound when microphones are positioned at the center or edge, a finite element simulation was conducted using COMSOL Multiphysics software, as depicted in Fig. 2(a). The SD, containing an internal air cavity, is fully submerged in water. The simulation model consists of three domains: the photosensitive resin shell of the SD (whose shell thickness is 1 mm), the internal air cavity, and the surrounding water domain. The material properties used in the simulation are: water (density 998 kg/m^3, sound speed 1484 m/s), air (density 1.21 kg/m^3, sound speed 343 m/s), and photosensitive resin (density 1200 kg/m^3, Young's modulus 2 GPa, Poisson's ratio 0.35).

Acoustically nonreflective perfectly matching layers (PMLs) with a thickness of 20 mm are set on the sides and bottom of the water domain, ensuring no echoes distort the acoustic pressure measurements. The water-air interface

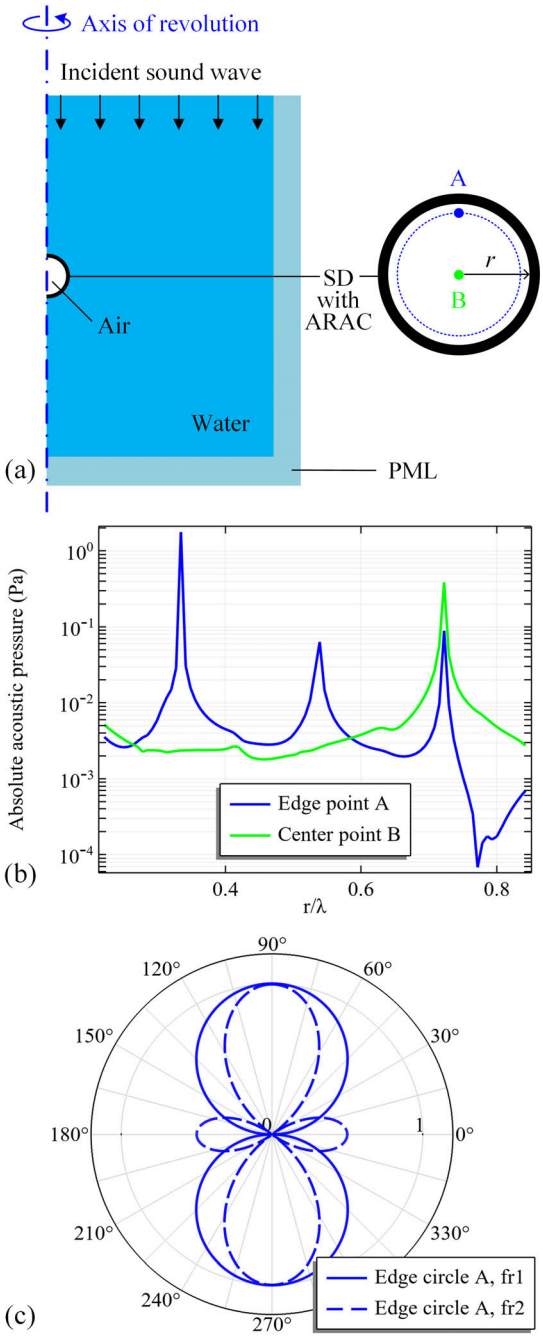

Fig. 2. Frequency response simulation of an SD containing a spherical ARAC. (a) Simulation setup. (b) Received acoustic pressure spectra at different points in the ARAC. (c) Acoustic receiving directivity pattern.

at the cavity boundary is modeled using acoustic-structure interaction physics, considering both acoustic pressure and structural displacement. Incident sound waves, with a pressure amplitude of 1 Pa and different frequencies, are transmitted vertically from the water's upper surface to the lower bottom.

The model was meshed using quadratic tetrahedral elements with a maximum element size of $\lambda_{\min}/10$, where $\lambda_{\min}$ corresponds to the shortest wavelength in the simulation frequency range. This ensures at least ten elements per wavelength for accurate wave propagation modeling.

To investigate the frequency response characteristics for SDs of different sizes, a dimensionless parameter r/λ (where r is the cavity radius and λ is the wavelength of sound in air) was introduced in the frequency domain study. Given that frequency f is inversely proportional to wavelength λ, since $f = c/\lambda$ where c is the speed of sound in air, the ratio r/λ represents the equivalent frequency of sound waves received by SDs of different sizes. The simulation swept over r/λ values from 0.2 to 0.85, which effectively normalized the frequency response for different cavity sizes.

The frequency sweeping results of points A and B are shown in Fig. 2(b). At point A, the frequency response curve includes three peaks corresponding to the first three resonance frequencies of the cavity when r/λ is 0.2–0.85; at point B, only the peak of the third resonance mode appears in the same range of r/λ. As shown in Fig. 2(c), there are significant differences in the directivity of the SD at different frequencies. At the frequency f_{r1}, the SD exhibits a concentrated directional receiving pattern, particularly achieving maximum response at 90° and 270° angles. At the frequency f_{r2}, in addition to strong responses at 90° and 270°, notable responses are also observed at 0° and 180° angles, although these are slightly lower than the two peak values. In comparison to point B, the resonance cavity at point A can fully respond to the first three resonance frequencies, f_{r1}, f_{r2}, and f_{r3}. Positioning the microphone at the edge of the SD is, therefore, considered advantageous for better capturing and amplifying leak noise signals.

III. Leak Detection Performance of SD Prototypes With Different Sizes of ARACs

Five leak detection spheres, serving as prototypes for future SDs with diameters of Φ96, Φ50, Φ28, Φ16, and Φ11.42 mm, were meticulously designed and cabled to facilitate the detection of small pipeline leaks. These specific diameters were selected to ensure their resonance frequencies would effectively cover the characteristic frequency band of pipeline leak sounds ranging from 100 to 5000 Hz. Microphones were positioned at the edge of the cavities of these spheres to explore the SD's acoustic responses with various cavity sizes and acoustic pressure distribution modes. According to Fig. 1(c), the theoretical characteristic frequencies of the above five SDs' ARACs are as follows f_{r1}: 2368, 4548, 8121, 14 213, and 19 913 Hz, f_{r2}: 3803, 7302, 13 040, 22 820, and 31 972 Hz, and f_{r3}: 5113, 9818, 17 533, 30 683, and 42 988 Hz.

As depicted in Fig. 3, each SD consists of a spherical shell and potting tube fabricated from light-curing resin using 3-D printing techniques. A microphone is affixed at the sphere's edge and connected to a potting circuit board for signal amplification and electromagnetic interference reduction. Both the spherical shell and the potting tube are sealed with epoxy resin adhesive to ensure waterproofing and pressure resistance.

The experimental setup for the pipeline leak test, as illustrated in Fig. 4, includes a liquid-filled pipeline integrated with a signal acquisition system and a leak detection SD. The pipeline, sealed at both ends by flange blind plates, is 8 m long with an outer diameter of 219 mm and a wall

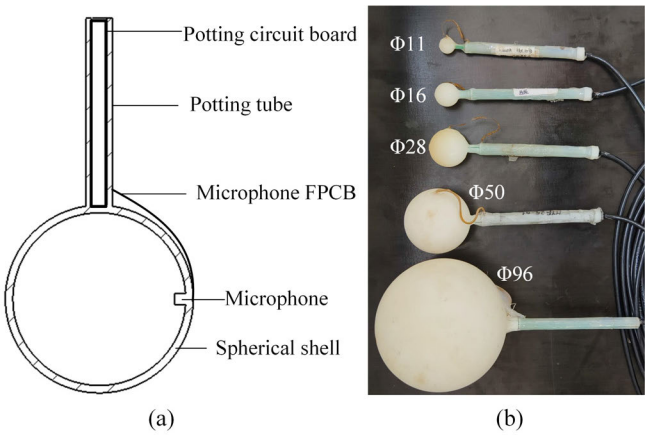

Fig. 3. Leak SD prototypes with different sizes. (a) Cross section and component layout. (b) Photographs of five SD prototypes.

thickness of 6 mm. A quick-opening blind plate, equipped with a pressure-resistant waterproof joint, facilitates the insertion of the leak detection sphere and the seamless connection of the waterproof cable from the sphere to a signal acquisition card. Threaded holes located in the pipeline's midsection enable the simulation of leaks. A steel wire rope running over pulleys is connected to the SD's base, which features a hollow semi-cylindrical structure matching the pipeline's interior curvature. Inside this hollow base, steel ball counterweights are used to maintain the device's stability at the bottom of the water-filled pipeline. The movement of the leak SD, controlled via the steel wire rope, enables precise positioning near the simulated leak point.

The signal acquisition system comprises the SD prototype connected via waterproof cables to an acquisition card and a PC running LabVIEW software, which controls data collection at a sampling rate of 500 kHz. The leak test pressure at the beginning is 0.2 MPa, and the leak aperture is 1 mm in diameter. Once the leak begins, the pressure gradually decreases to zero. Each sphere was tested three times to assess leak detection effectiveness by comparing SPLs near the resonance frequency. Comprehensive analyses were performed to evaluate the impact of varying resonant frequencies and cavity sizes on leak detection sensitivity.

Guo's research [29] suggests that the acoustic signal from leaks is a type of broadband noise with varying attenuation characteristics within a specific frequency band. Above the cutoff frequency, the leak-induced acoustic signal experiences attenuation, while within the bandwidth below the cutoff frequency, the amplitude of the leak acoustic signal remains high and stable. Huang et al. [25] and Xu et al. [27] determined that the high-energy acoustic frequency band generated by pipeline leaks falls within the range of 100–5000 Hz, in the bandwidth range beyond which the leak sound significantly attenuates.

Considering the bandwidth of the leak sound signal, the resonant frequencies f_{r1}, f_{r2}, and f_{r3} of the Φ96 mm leak detection sphere are 2380, 3823, and 5159 Hz, respectively, and fall within the high-energy band of leak sounds. To analyze these signals, the short-time Fourier transform (STFT) was applied to the acoustic data collected by the Φ96 mm sphere, as depicted in Fig. 5. The STFT analysis shows that throughout the leak process, significant energy concentrations occur near the frequencies f_{r1}, f_{r2}, and f_{r3}, aside from the background noise in the low-frequency range. These characteristic frequencies exhibit a high-energy response at the onset and weakening process of the leak, with the energy gradually diminishing thereafter. This pattern indicates that the leak-induced sound is intense at the beginning and gradually diminishes as the pressure decreases until it becomes undetectable. The STFT analysis effectively confirms the SD's capability in detecting subtle and continuous leaks.

The amplitude changes at the three resonant frequencies extracted from the STFT analysis indicate that in the first 90 s of the leak, the sensitivity of f_{r1} is higher than that of f_{r2} and f_{r3}. Notably, between 10 and 30 s into the leak, differential changes occur in the amplitudes at the three frequencies: f_{r1} and f_{r2} decrease, while f_{r3} slightly increases, which is likely due to initial pressure fluctuations and a resultant shift in the leak sound spectrum toward higher frequencies. After 50 s into the leak, the amplitudes at all three frequencies continue to decline, with f_{r3} experiencing the most significant drop, demonstrating that as the pressure further decreases, the high-frequency components of the leak signal are the first to diminish. Hence, different resonant frequencies demonstrate varying applicability under different pressure conditions in water pipelines. Specifically, f_{r1} has the highest sensitivity to leak sound. During significant leak sound, f_{r3} exhibits greater sensitivity than f_{r2}, while f_{r2} shows higher sensitivity than f_{r3} during minor leak sound.

To evaluate the leak detection capabilities of SDs of different sizes, amplitude changes at f_{r1} during the leak process were analyzed for the five sizes of SDs: Φ96, Φ50, Φ28, Φ16, and Φ11.42 mm. As shown in Fig. 6, SDs of all sizes are able to detect leak events, but the detection sensitivity decreases with the reduction in the SD diameter. This phenomenon is primarily related to the resonance frequency of the cavity; as previously analyzed [refer to Fig. 1(c)], smaller cavity sizes correspond to higher resonance frequencies. An increase in frequency, however, typically results in decreased energy in the pipeline leak sound, thus reducing the sensitivity of SDs with smaller cavities. It is, therefore, advisable to consider the compatibility between the pipe diameter and the SD diameter when designing the SD, aiming to maximize the SD diameter to enhance leak detection sensitivity.

To further quantitatively evaluate the detection capability and establish statistical confidence bounds of the SD system, additional experiments were conducted using the Φ96 mm SD prototype under controlled conditions. The experimental procedure first established a baseline by measuring the background noise with the leak hole sealed. Subsequently, leak detection tests were performed with four different leak apertures (0.4, 0.6, 0.8, and 1.0 mm) under an initial pressure of 0.2 MPa, recording complete acoustic signals throughout the entire leak process.

The energy variation at f_{r1} was extracted through spectral analysis for each measurement. Given the normal distribution characteristics of background noise, a detection threshold

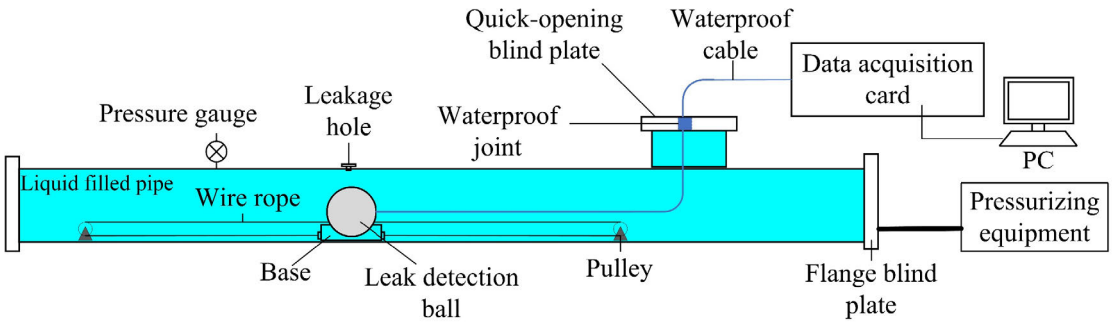

Fig. 4. Pipeline leak test system.

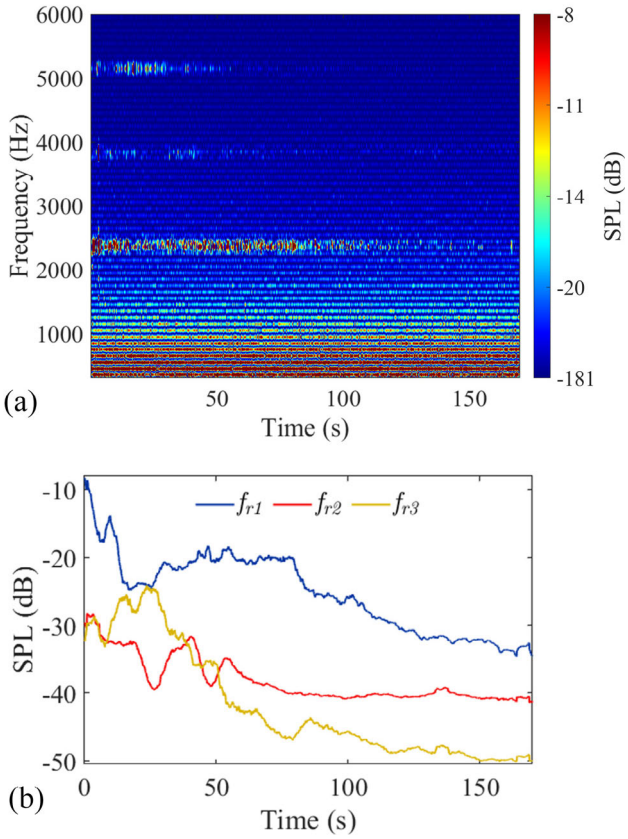

Fig. 5. Different modes of leak sound detected by the Φ96 SD prototype in the process of decreasing pipeline leak. (a) Time-frequency analysis. (b) Amplitude change process of three resonant frequencies.

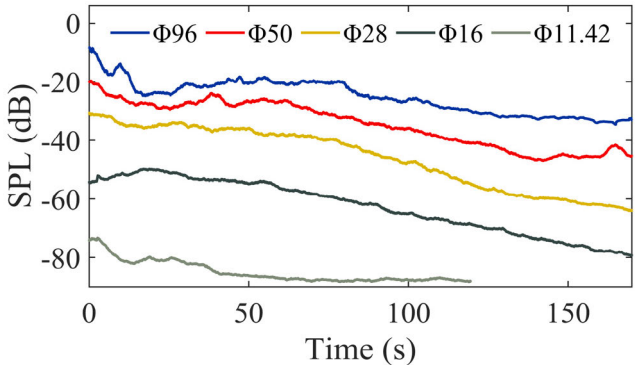

Fig. 6. Amplitude change process of the resonant frequency f_{r1} of five SD prototypes.

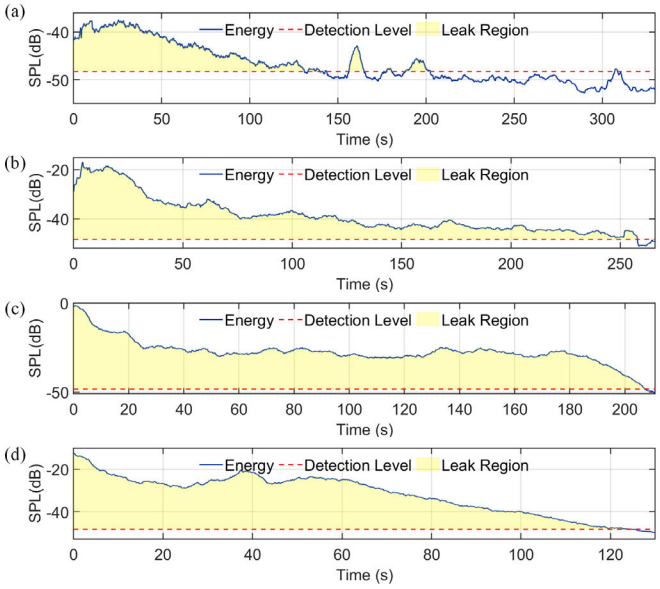

Fig. 7. Leak detection results at different leak apertures during the entire leak process. (a) 0.4 mm leak aperture. (b) 0.6 mm leak aperture. (c) 0.8 mm leak aperture. (d) 1.0 mm leak aperture.

was established using the three-sigma rule, where signals exceeding $\mu + 3\sigma$ (μ and σ representing the mean and standard deviation of background noise energy, respectively) were considered positive detections, corresponding to a 99.7% confidence level. As shown in Fig. 7, the total leak duration exhibits an inverse relationship with aperture size—the 0.4 mm aperture maintains a leak duration of approximately 320 s, while the 1.0 mm aperture sustains only 120 s due to faster pressure dissipation through larger openings.

Under the initial pressure of 0.2 MPa, distinct acoustic signatures were observed across different apertures. The 0.8 mm aperture generated the highest SPL of approximately 0 dB, followed by 0.6 and 1.0 mm apertures at around −20 dB, while the 0.4 mm aperture produced a relatively lower level of −40 dB. As the pressure gradually decreased during the leak process, all energy curves demonstrated declining trends, with larger apertures exhibiting steeper drops due to more rapid pressure dissipation rates. Smaller apertures maintained

TABLE I
STATISTICAL ANALYSIS OF LEAK DETECTION UNDER DIFFERENT APERTURES WITH 99.7% CONFIDENCE LEVEL

Aperture	Mean Leak Power	Leak Power STD	Mean SNR	Detection Rate
0.4mm	-43.66 dB	3.35 dB	4.64 dB	50.54%
0.6mm	-38.55 dB	7.42 dB	9.75 dB	96.92%
0.8mm	-27.22 dB	6.58 dB	21.08 dB	98.14%
1.0mm	-31.36 dB	8.78 dB	16.94 dB	95.88%

(a) (b)

Fig. 8. Actual image of leakage state. (a) 0.8 mm aperture leakage. (b) 1.0 mm aperture leakage.

relatively stable energy levels for extended periods owing to their slower pressure release characteristics.

Statistical analysis of the f_{r1} energy level throughout the entire leak process yielded comprehensive performance metrics, as summarized in Table I. With the detection threshold set at -48.30 dB based on background noise analysis, the 0.8 mm aperture achieved optimal performance with a mean SNR of 21.08 dB and a detection rate of 98.14%. The 0.6 and 1.0 mm apertures demonstrated comparable performance, both achieving detection rates exceeding 95% with mean SNRs of 9.75 and 16.94 dB, respectively. Even the smallest 0.4 mm aperture achieved a detection rate of 50.54% with a mean SNR of 4.64 dB. These results demonstrate that at a 99.7% confidence level, the system exhibits robust detection capability with detection rates exceeding 95% for leak apertures ranging from 0.6 to 1.0 mm.

Notably, the detection sensitivity for the 0.8 mm leak aperture exceeded that of the 1.0 mm aperture. This observation necessitates further investigation into the underlying fluid dynamic mechanisms. Through experimental observation, it was found that the leakage flow velocity significantly impacts the fluid's transition between turbulent and laminar states. Under identical pressure conditions, the 0.8 mm aperture was more prone to inducing turbulent flow, which generates stronger acoustic signals compared to the more stable laminar flow typically observed with the 1.0 mm aperture. This distinction is visually documented in Fig. 8, where the flow through the 0.8 mm aperture manifests as a white, opaque jet characteristic of turbulent flow, while the flow through the 1.0 mm aperture appears as a darker, partially transparent stream indicative of laminar flow. This fluid dynamic behavior directly influences the detection sensitivity, with turbulent flow producing more detectable acoustic signatures than laminar flow conditions.

IV. DESIGN OF SD WITH ARAC FOR FIELD APPLICATION

The overall design of the field application SD was driven by three key requirements: 1) maximizing ARAC sensitivity while

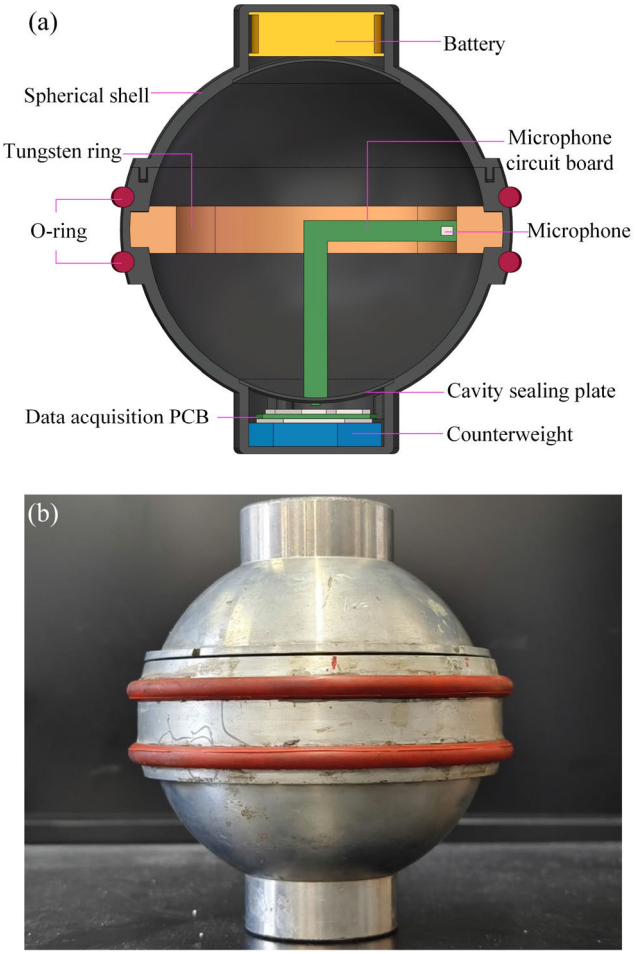

Fig. 9. Developed SD for field pipeline leak detection. (a) Internal structure of the SD. (b) Photograph of the SD.

maintaining structural integrity; 2) ensuring stable rolling motion and minimal mechanical noise, and 3) achieving reliable operation under high-pressure conditions. Each component's design and arrangement were optimized to meet these requirements while addressing the practical constraints of field deployment.

In order to address the needs of on-site pipeline leak detection, a new type of SD is designed and developed, as shown in Fig. 9. The SD structure incorporates an aluminum alloy spherical shell, O-rings, and tungsten ring counterweights. Structurally, the SD is divided into three main areas: 1) the equipment areas, located at the top and bottom and containing the battery and data acquisition printed circuit board (PCB), respectively; 2) the middle part of the sphere contains a spherical cavity, isolated from the equipment areas by two cavity sealing plates; and 3) copper counterweights in the bottom area to align the sphere's center of gravity with its geometric center and balance the weight distribution of equipment.

According to Lin et al. [30], a sphere will maintain rolling about the axis with larger rotational inertia during flow-driven motion. Based on this principle, a tungsten ring counterweight is installed at the sphere's equator to achieve a ratio of 1.25 between the rotational inertia about the vertical

axis (z-axis) and that about the horizontal axis (x-axis). This configuration ensures that the SD rolls along its equatorial axis, resulting in contact points concentrated only at the SD's equatorial edge against the pipe bottom. Soft silicone O-rings are, therefore, installed on either side of the equator for damping and shock absorption purposes, avoiding the need to cover the entire spherical shell with damping material, which would increase the transmission of leak sounds into the SD.

In the electronic system, the microphone circuit board is mounted between the bottom sealing plate and the tungsten ring. When the SD is far from the leak point, and the leak sound propagates along the pipeline axis, the leak sound source is bound to be in the direction perpendicular to the rotation axis of the SD. Considering the sensitivity of f_{r1} and f_{r2} to leak sound sources, the microphone is optimally placed at the equator's edge, rather than at the poles, to enhance its ability to capture leak sounds during rotation around the fixed axis. The data acquisition PCB, located at the bottom of the equipment area, is connected to the battery and microphone circuit board via wires. Data acquisition PCB includes a microcontroller unit (MCU) unit, a triaxial accelerometer, a TransFlash (TF) card, and a pulse-density modulation (PDM) signal demodulator, which is responsible for collecting accelerometer data and decoding the microphone's PDM output signals. Ultimately, the data are stored on the TF card in file format, with an accelerometer sampling rate of 200 Hz and an audio signal sampling rate of 8 kHz.

Research by Guo et al. [24] demonstrates that optimal hydraulic thrust acting on the SD is achieved within the pipeline when the ratio of the SD's outer diameter to the pipeline's inner diameter falls between 0.6 and 0.8. Through finite element analysis and experimental validation, this ratio range was found to provide the optimal balance between detection performance and operational requirements. A smaller ratio ($<$0.6) would result in unstable rolling motion and reduced sensitivity to leak signals, while a larger ratio ($>$0.8) would increase the risk of pipeline obstruction and excessive friction with the pipe wall. In order to balance the need for significant thrust and good passability, this ratio was set at 0.69 for an experimental field pipeline with an inner diameter of 193 mm, yielding an SD outer diameter of 133 mm. Additionally, to maintain adequate wall thickness for pressure resistance and maximize the resonant cavity volume, the cavity diameter was set at 116 mm. Finite element simulations indicate that for an SD of this internal diameter, the f_{r1}, f_{r2}, and f_{r3} are 2095, 3384.6, and 4279.9 Hz, respectively.

V. Field Experiments of Leak Detection

Fig. 10 illustrates the layout of the experimental field pipeline used for the leak detection test of the developed SD. The pipeline's total length is 657.46 m, and its internal and external diameters are 193 and 219 mm, respectively. Several mileage points are marked in Fig. 10. The experiment starts at the SD transceiver platform, marked near the 0 m position, which serves as the control and data initialization hub. The pipeline consists of multiple straight sections and elbows that realize directional changes. Following the flow direction, the pipeline starts with a straight segment measuring 135.80 m from the SD transceiver platform. After passing through the elbows at 168.1, 301.9, and 308.79 m, the pipeline extends to the leak hole, which is located at 416.89 m and has a diameter of 1 mm. Indentations are present on the pipeline's wall, 5 m upstream and downstream of the leak hole. After the leak point, the pipeline goes through a series of elbows and short sections that are cumulatively approximately 80 m before returning via a long straight section to the SD transceiver platform.

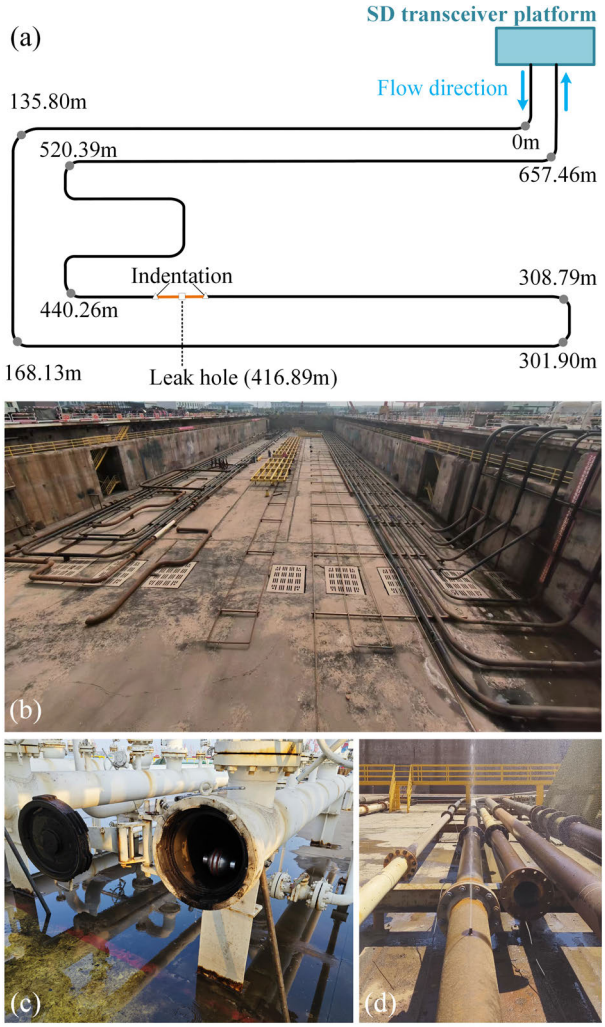

Fig. 10. Field pipeline leak detection experiment. (a) Pipeline layout. (b) Photograph of field pipeline. (c) SD transceiver platform. (d) Photograph of leak point.

Before the experiment, the SD was activated and initialized at the SD transceiver platform. Subsequently, the SD was placed into the launch tube, as depicted in Fig. 10(c). Operators pushed the SD into the pipeline using a push rod, and then closed the pipeline valve to seal the pipe system. The water flow rate and pressure were then set to the predetermined experimental parameters. Once everything was prepared, the valve was opened to launch the SD. The SD then traveled through the entire pipeline system, propelled by the water flow,

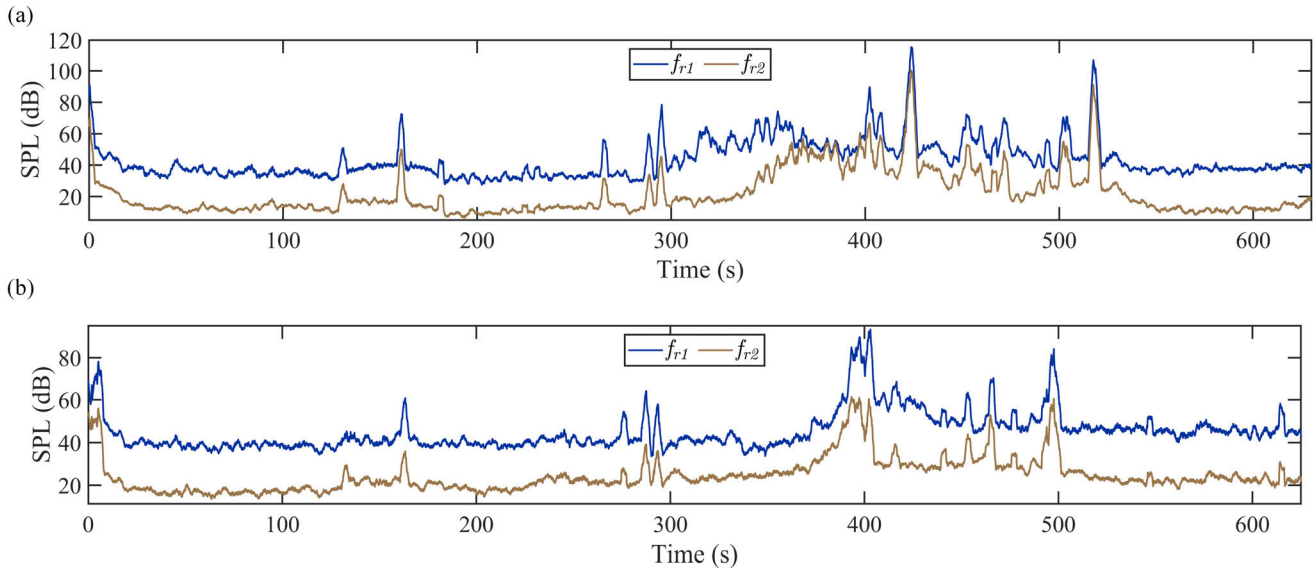

Fig. 11. Amplitude curves the resonance frequencies f_{r1} and f_{r2} under different experimental conditions. (a) 1 MPa and 1 m/s. (b) 0.5 MPa and 1 m/s.

and ultimately returned to the transceiver platform for retrieval.

Experiments were conducted with a pipeline flow speed of 1 m/s, with high pressure of 1 MPa and low pressure of 0.5 MPa. The acoustic signals recorded throughout the SD's journey under both experimental conditions were analyzed using STFT, from which amplitude curves at different frequencies were extracted. The microphone sampling rate was set at 8 kHz, enabling undistorted capture and recovery of signals below 4000 Hz in accordance with the Nyquist Sampling Theorem. The experiments, therefore, primarily focused on analyzing the amplitude changes at f_{r1} and f_{r2} throughout the duration. The amplitude of the third resonance frequency $f_{r3} = 4279.9$ Hz was not analyzed and extracted.

As depicted in Fig. 11 the amplitude values of the two resonance frequencies, f_{r1} and f_{r2}, are very low within the first 300 s of the experiment when the SD is in the pipeline sections without leak. Amplitude peaks were, however, observed at 130, 160, and 300 s, corresponding to the SD's collisions with pipeline elbows. From 300 to 390 s, while the SD passes through the straight pipeline section containing the leak, a significant increase in amplitude values is observed. Under the high-pressure condition of 1 MPa, f_{r1} exhibits an earlier increase in energy, indicating its higher sensitivity to leak sounds. Compared to f_{r1}, which shows an earlier increase in energy, f_{r2} only demonstrates a significant rise in amplitude as it approaches the leak site, indicating its slightly lower sensitivity, as previously discussed. Under the lower pressure condition of 0.5 MPa, both f_{r1} and f_{r2} show a notable rise in energy between 370 and 390 s, demonstrating the SD's successful detection of the leak signal despite lower leak sound and limited propagation distance. Between 390 and 430 s, under both pressure conditions, two high-energy peaks appear in the amplitude curves due to the SD's collisions with pipeline wall indentations. From 430 to 500 s, the SD navigates through continuous elbows, resulting in multiple amplitude fluctuations

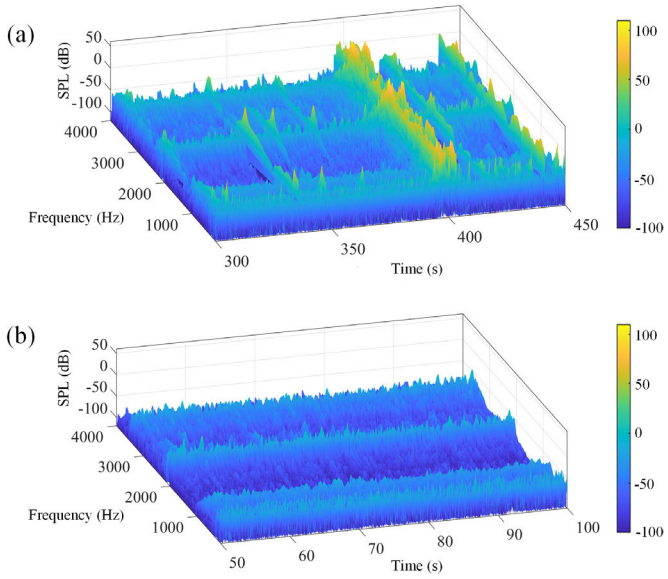

Fig. 12. STFT of Acoustic signal segments at 0.5 MPa and 1 m/s (a) with leak and (b) without leak.

from frequent collisions. After 500 s, the amplitude values gradually stabilize under both experimental pressure conditions until the SD reaches the endpoint and marks the completion of the rolling detection process.

For assessing the SD's capability to differentiate between leak and nonleak conditions, 3-D energy spectrum graphs were plotted under conditions of 0.5 MPa pressure and a flow speed of 1 m/s, as shown in Fig. 12. Fig. 12(a) displays the energy spectrum of the SD from 300 to 450 s, during its passage over the leak pipeline section, while Fig. 12(b) presents the energy spectrum for a nonleak straight pipeline segment from 50 to 100 s. In the leakage segment, the energy levels at 2095 Hz (f_{r1}) and 3384 Hz (f_{r2}) are notably

higher compared to the nonleak segment. Particularly between 370 and 390 s, there is a significant rise in SPLs at f_{r1} and f_{r2}, with no similar changes observed at other frequencies. These results distinctly demonstrate the high sensitivity and excellent frequency selection amplification of the SD's resonant cavity to leak signals, thereby confirming its effectiveness in practical leak detection applications in field pipelines in the state of rolling forward.

To establish a formal criterion for leak detection and effectively distinguish between leak signals and mechanical impacts, a systematic signal processing algorithm has been developed and implemented. The algorithm consists of two main stages: mechanical impact removal and leak event identification.

A. Step 1: Removing Mechanical Impact Signals

The first stage processes the SPL curves within specific frequency ranges to eliminate mechanical impact influences. This process comprises the following key steps.

1) Wavelet Decomposition: We use the discrete wavelet transform (DWT) to decompose the original signal into approximation coefficients and detail coefficients. For decomposition level N, the approximation coefficient a_N represents the low-frequency part of the signal, while the detail coefficients $d_1, d_2, \ldots, d_N$ represent the high-frequency parts at different scales.

2) Spike Detection: On the approximation coefficients, we apply a sliding window method to detect spikes. For a window $[t, t + \Delta t]$, we calculate the difference

$$D(t) = |a_N(t + \Delta t) - a_N(t)|.$$

If $D(t)$ exceeds a predetermined threshold T_s, the window is marked as containing a spike.

3) Curve Fitting: For detected spike regions $[t_{\text{start}}, t_{\text{end}}]$, we use a quadratic interpolation method to reconstruct the signal. We calculate the average slopes before and after the spike

$$m_{\text{before}} = \frac{a_N(t_{\text{start}}) - a_N(t_{\text{start}} - w)}{w}$$
$$m_{\text{end}} = \frac{a_N(t_{\text{end}} + w) - a_N(t_{\text{end}})}{w}$$

where w is the window size used for calculating slopes. Then, we use these slopes to reconstruct the signal through slope interpolation.

First, we perform linear interpolation of slopes

$$\text{slope}(t) = m_{\text{pre}} + \frac{(m_{\text{end}} - m_{\text{before}})(t - t_{\text{start}})}{t_{\text{end}} - t_{\text{start}}}.$$

Then, we reconstruct the signal iteratively

$$a'_N(t + 1) = a'_N(t) + \text{slope}(t), \quad \text{for } t \in [t_{\text{start}}, t_{\text{end}}]$$

where $a'_N(t_{\text{start}}) = a_{N(t_{\text{start}})}$.

4) Signal Reconstruction: Using the modified approximation coefficients and the original detail coefficients, we reconstruct the signal through inverse DWT.

B. Step 2: Leak Detection and Localization

Following mechanical impact removal, the algorithm implements the following method for leak detection and localization.

1) Background Noise Analysis: We select a known leak-free time period $[t_{\text{bg\_start}}, t_{\text{bg\_end}}]$ to analyze background noise. Calculate the mean μ_{bg} and standard deviation σ_{bg} of the signal within this period.

2) Adaptive Threshold Setting: We set the leak detection threshold T_l as

$$T_l = \mu_{\text{bg}} + \alpha \cdot \sigma_{\text{bg}}$$

where α is an adjustable parameter, typically ranging from 3 to 6.

3) Leak Event Identification: We scan the entire signal, and if the signal intensity continuously exceeds the threshold T_l for a duration of $\Delta t_{\min}$, we mark it as a potential leak event.

4) Multifrequency Validation: To improve detection reliability, we repeat the above process in multiple characteristic frequency ranges. We only confirm the existence of a leak when multiple frequency ranges indicate its presence.

Fig. 13 illustrates the processing results and leak detection outcomes under different experimental conditions. Compared to the unprocessed signals shown in Fig. 11, the algorithm effectively mitigates the high-energy fluctuations caused by mechanical impacts while preserving the underlying leak-related acoustic features. The detected leak regions, highlighted in yellow, exhibit distinct characteristics under different pressure conditions. Under 1 MPa pressure, the detected leak region demonstrates a broader temporal extent compared to the 0.5 MPa condition, which aligns with theoretical expectations as higher pressure generates stronger leak signals with enhanced propagation characteristics. This algorithmic implementation provides quantitative validation of the SD's capability as a reliable leak detection system, effectively differentiating between genuine leak events and mechanical disturbances under varying operational conditions.

VI. Limitations and Future Work

A. Technical Limitations and Practical Challenges

While the developed SD system demonstrates promising capabilities in pipeline leak detection, several limitations and challenges need to be acknowledged. The current design faces pipe diameter constraints, as the SD's size must be carefully balanced between detection sensitivity and pipeline passability. For pipelines with diameters significantly different from our test conditions (193 mm), redesign and reoptimization of the ARAC would be beneficial.

The system's performance is also pressure-dependent, with detection sensitivity varying between high (1 MPa) and low (0.5 MPa) pressure conditions. This pressure sensitivity presents challenges in pipelines with fluctuating operational pressures. Additionally, complex pipeline configurations, such as multiple consecutive elbows or sharp bends, can affect the SD's movement stability and signal quality.

In practical applications, the presence of debris or deposits in operational pipelines may impact the SD's rolling behavior and acoustic measurements. The current power and storage

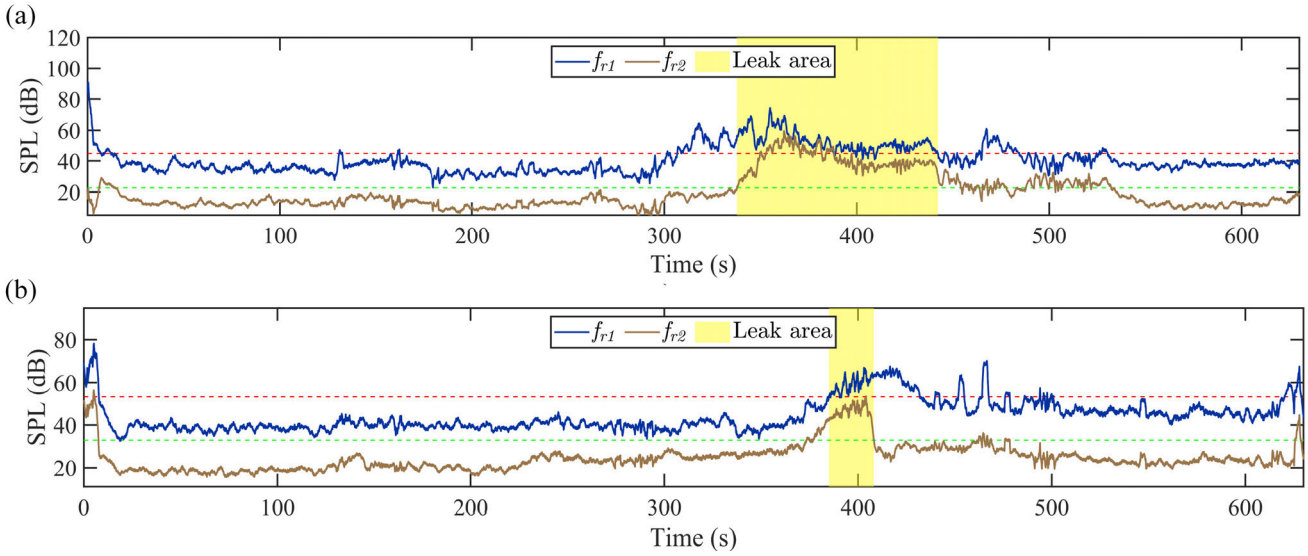

Fig. 13. Processed amplitude curves and leak areas at resonance frequencies f_{r1} and f_{r2} under different experimental conditions. (a) 1 MPa and 1 m/s. (b) 0.5 MPa and 1 m/s.

capabilities also limit continuous operation time, particularly in long pipeline systems. Processing the large volumes of acoustic data collected during inspection runs, furthermore, poses computational challenges, especially for real-time analysis and immediate leak detection.

B. Future Improvements and Research Directions

Several potential improvements could enhance the SD system's capabilities and practical applicability. The development of deep learning-based algorithms could automate the analysis of acoustic signatures, potentially improving both detection accuracy and computational efficiency. Such algorithms could better differentiate between leak signals and other pipeline noises, reducing false positives.

Power management optimization through advanced battery technologies and energy-efficient components could extend operational duration. Integration of multiple sensor types, such as pressure sensors, could provide complementary data for more robust leak detection. Real-time data transmission capabilities could enable immediate leak alerts, though this would require addressing challenges in underwater communication.

Future research should explore the acoustic generation and propagation mechanisms in operational pipelines, particularly focusing on the interaction between leak flow and high-speed main pipeline flow. Our field experiments revealed that leak sounds could propagate several tens of meters from the leak point, a phenomenon not observed in laboratory tests with stagnant fluid in the pipeline. This extended propagation range suggests that the interaction between high-velocity pipeline flow and leak jet flow may generate additional acoustic signatures or enhance sound propagation. Understanding these fluid-acoustic coupling mechanisms through detailed numerical simulations and experimental studies could provide valuable insights for optimizing detection sensitivity and expanding the detection range of the SD system.

These improvements would advance the practical application of SD technology in pipeline infrastructure maintenance and monitoring.

VII. Conclusion

Using the ARAC, the SD demonstrates high sensitivity and frequency-selective detection for continuous minor leaks in field pipelines. This study analyzes and validates the relationship between leak detection sensitivity and factors such as cavity size and acoustic resonance modes via finite element simulations and stationary water-filled pipeline leak detection experiments. Field tests were conducted to validate the leak detection capability of the ARAC-based SD in operational pipelines. The following conclusions can be drawn.

1) Larger SDs and ARACs featuring lower characteristic frequencies can effectively capture the low-frequency, high-energy components of broadband leak signals, thereby enhancing the SD's leak detection sensitivity. When the ARAC's diameter exceeds 96 mm, its first three modal frequencies can cover the high-energy frequency band of leak sounds. Among these, f_{r1} shows the highest sensitivity to leaks; f_{r3} is more sensitive than f_{r2} to significant leaks; and f_{r2} exhibits greater sensitivity than f_{r3} to minor leaks.
2) Based on these findings, the size and basic layout of the leak SD are determined, resulting in an optimized SD design featuring an ARAC with a microphone positioned at the edge. The primary purpose of maximizing the SD's size is specifically to enlarge the ARAC. Components and counterweights are meticulously arranged to ensure stable rolling of the SD around its designed axis. The SD contacts the pipeline walls only with two O-rings at its equator, eliminating the need to cover the entire SD shell with damping material, and thus, enhancing the transmission of leak sounds into the SD.
3) The developed SD effectively detects leaks while rolling forward in pipelines under operational pressures of 1 and

0.5 MPa with a leak aperture of 1 mm. Under a 1 MPa pressure condition, an onset of increase in amplitude is observed at different times for f_{r1} and f_{r2} before the SD reaches the leak point. At 0.5 MPa, a significant rise in amplitude is observed only at the resonant frequencies, which demonstrates the critical role of the ARAC in enhancing the SD's leak detection capability.

4) The proposed signal processing algorithm, combining wavelet decomposition and adaptive thresholding, effectively distinguishes leak signals from mechanical impacts and background noise. The algorithm achieves reliable leak detection with detection rates exceeding 95% for leak apertures ranging from 0.6 to 1.0 mm under controlled conditions, demonstrating robust performance in practical applications.
5) Quantitative analysis of the detection results under various experimental conditions reveals that the system maintains effective detection capability even under challenging field conditions, with the algorithm successfully identifying leak events while filtering out interference from pipe wall collisions and other environmental noise. The systematic approach to signal processing and analysis provides a foundation for future improvements in automated leak detection systems.

REFERENCES

[1] F. Wang, W. Lin, Z. Liu, S. Wu, and X. Qiu, "Pipeline leak detection by using time-domain statistical features," *IEEE Sensors J.*, vol. 17, no. 19, pp. 6431–6442, Oct. 2017, doi: 10.1109/JSEN.2017.2740220.

[2] W. Li et al., "Development of systems for detection, early warning, and control of pipeline leakage in drinking water distribution: A case study," *J. Environ. Sci.*, vol. 23, no. 11, pp. 1816–1822, Nov. 2011, doi: 10.1016/s1001-0742(10)60577-3.

[3] J. Xu et al., "Low-cost, tiny-sized MEMS hydrophone sensor for water pipeline leak detection," *IEEE Trans. Ind. Electron.*, vol. 66, no. 8, pp. 6374–6382, Aug. 2019, doi: 10.1109/TIE.2018.2874583.

[4] J. Yuan, W. Mao, C. Hu, J. Zheng, D. Zheng, and Y. Yang, "Leak detection and localization techniques in oil and gas pipeline: A bibliometric and systematic review," *Eng. Failure Anal.*, vol. 146, Apr. 2023, Art. no. 107060, doi: 10.1016/j.engfailanal.2023.107060.

[5] L. Zhao, Z. Cao, and J. Deng, "A review of leak detection methods based on pressure waves in gas pipelines," *Measurement*, vol. 236, Aug. 2024, Art. no. 115062, doi: 10.1016/j.measurement.2024.115062.

[6] J. Li, Q. Zheng, Z. Qian, and X. Yang, "A novel location algorithm for pipeline leakage based on the attenuation of negative pressure wave," *Process Saf. Environ. Protection*, vol. 123, pp. 309–316, Mar. 2019, doi: 10.1016/j.psep.2019.01.010.

[7] V. Q. C. Tran, D. V. Le, D. R. Yntema, and P. J. M. Havinga, "A review of inspection methods for continuously monitoring PVC drinking water mains," *IEEE Internet Things J.*, vol. 9, no. 16, pp. 14336–14354, Aug. 2022, doi: 10.1109/Jiot.2021.3077246.

[8] M. I. M. Ismail et al., "A review of vibration detection methods using accelerometer sensors for water pipeline leakage," *IEEE Access*, vol. 7, pp. 51965–51981, 2019, doi: 10.1109/ACCESS.2019.2896302.

[9] N. Lalam et al., "Pilot-scale testing of natural gas pipeline monitoring based on phase-OTDR and enhanced scatter optical fiber cable," *Sci. Rep.*, vol. 13, no. 1, p. 14037, Aug. 2023, doi: 10.1038/s41598-023-41338-4.

[10] Y. Yang, S. Zhou, F. Hao, J. Zhining, and G. Q. Wang, "Signal processing method of ϕ-OTDR technology in early warning and leakage positioning of water pipelines," *Laser Optoelectron. Prog.*, vol. 55, no. 4, 2018, Art. no. 040607.

[11] X. Zhou et al., "Hybrid B-OTDR/ϕ-OTDR for multi-parameter measurement from a single end of fiber," *Opt. Exp.*, vol. 30, no. 16, p. 29117, Aug. 2022, doi: 10.1364/oe.463127.

[12] P. Clément, R. Gabet, V. Lanticq, and Y. Jaouën, "B-OTDR solution for independent temperature and strain measurement in a single acquisition," *J. Lightw. Technol.*, vol. 39, no. 18, pp. 6013–6020, Sep. 15, 2021, doi: 10.1109/JLT.2021.3088956.

[13] Z. Hu, S. Tariq, and T. Zayed, "A comprehensive review of acoustic based leak localization method in pressurized pipelines," *Mech. Syst. Signal Process.*, vol. 161, Dec. 2021, Art. no. 107994, doi: 10.1016/j.ymssp.2021.107994.

[14] K. Wu, "A survey on wireless in-pipe inspection robotics," *Int. J. Intell. Robot. Appl.*, vol. 8, no. 3, pp. 648–670, Sep. 2024, doi: 10.1007/s41315-024-00323-4.

[15] M. Coramik and Y. Ege, "Discontinuity inspection in pipelines: A comparison review," *Measurement*, vol. 111, pp. 359–373, Dec. 2017, doi: 10.1016/j.measurement.2017.07.058.

[16] Y. Long, S. Huang, L. Peng, W. Wang, S. Wang, and W. Zhao, "High-precision and four-dimensional tracking system with dual receivers of pipeline inspection gauge," *Appl. Sci.*, vol. 11, no. 8, p. 3366, Apr. 2021, doi: 10.3390/app11083366.

[17] G. Henrich, M. Taferner, and M. Huainig, "Simultaneous cableless video inspection of pipelines with integrated leak detection," in *Pipelines 2017: Condition Assessment, Surveying, Geomatics*, Phoenix, AZ, USA, 2017, pp. 584–595. [Online]. Available: <Go to ISI>://WOS:000425811100054.v

[18] T. Özaslan et al., "Autonomous navigation and mapping for inspection of penstocks and tunnels with MAVs," *IEEE Robot. Autom. Lett.*, vol. 2, no. 3, pp. 1740–1747, Jul. 2017, doi: 10.1109/Lra.2017.2699790.

[19] Y. Wu, K. Kim, M. F. Henry, and K. Youcef-Toumi, "Design of a leak sensor for operating water pipe systems," in *Proc. IEEE/RSJ Int. Conf. Intell. Robots Syst. (IROS)*, Sep. 2017, pp. 6075–6082. [Online]. Available: <Go to ISI>://WOS:000426978205100

[20] D. Kumar, D. Tu, N. Zhu, R. Shah, D. Hou, and H. Zhang, "The free-swimming device leakage detection in plastic water-filled pipes through tuning the wavelet transform to the underwater acoustic signals," *Water*, vol. 9, no. 10, p. 731, Sep. 2017, doi: 10.3390/w9100731.

[21] E. H. A. Duisterwinkel, E. Talnishnikh, D. Krijnders, and H. J. Wörtche, "Sensor motes for the exploration and monitoring of operational pipelines," *IEEE Trans. Instrum. Meas.*, vol. 67, no. 3, pp. 655–666, Mar. 2018, doi: 10.1109/TIM.2017.2775404.

[22] R. Fletcher and M. Chandrasekaran, "SmartBall: A new approach in pipeline leak detection," in *Proc. 7th Int. Pipeline Conf.*, vol. 2, Jan. 2008, pp. 117–133. [Online]. Available: <Go to ISI>://WOS:000265637000011

[23] T. Xu, Z. Zeng, X. Huang, J. Li, and H. Feng, "Pipeline leak detection based on variational mode decomposition and support vector machine using an interior spherical detector," *Process Saf. Environ. Protection*, vol. 153, pp. 167–177, Sep. 2021, doi: 10.1016/j.psep.2021.07.024.

[24] S. X. Guo, S. L. Chen, X. J. Huang, T. S. Xu, and S. J. Jin, "Design and application of a leak detector for submarine oil pipelines," *Modern Chem. Ind.*, vol. 35, pp. 182–186, Sep. 2015, doi: 10.16606/j.cnki.issn0253-4320.2015.09.046.

[25] X. Huang, Z. Li, J. Li, H. Feng, Y. Zhang, and S. Chen, "Acoustic investigation of high-sensitivity spherical leak detector for liquid-filled pipelines," *Appl. Acoust.*, vol. 174, Mar. 2021, Art. no. 107790, doi: 10.1016/j.apacoust.2020.107790.

[26] H. Xinjing et al., "Low-cost, high-sensitivity hydrophone based on resonant air cavity," *IEEE Sensors J.*, vol. 21, no. 6, pp. 7348–7357, Mar. 2021, doi: 10.1109/JSEN.2020.3048066.

[27] T. H. Xu, Z. M. Zeng, X. J. Huang, J. Li, S. L. Chen, and X. B. Rui, "Experimental investigation on acoustic characteristics of small leakages in metal water pipe for in-pipe inspections," in *Proc. IEEE IMTC*, May 2019, pp. 1048–1052, doi: 10.1109/I2MTC.2019.8827172.

[28] A. S. Papastefanou, P. F. Joseph, and M. J. Brennan, "Experimental investigation into the characteristics of in-pipe leak noise in plastic water filled pipes," *Acta Acustica United With Acustica*, vol. 98, no. 6, pp. 847–856, Nov. 2012, doi: 10.3813/aaa.918568.

[29] S. X. Guo, S. Liu, X. L. Liu, Z. M. Zeng, and S. J. Jin, "Research on acoustic characteristic of the near field inside the pipe for small leakage detection," *J. Electron. Meas. Instrum.*, vol. 30, no. 6, pp. 834–844, 2016, doi: 10.13382/j.jemi.2016.06.002.

[30] G. Lin et al., "Performance enhancements of the spherical detector for pipeline spanning inspection through posture stabilization," *Measurement*, vol. 165, Dec. 2020, Art. no. 108095, doi: 10.1016/j.measurement.2020.108095.

Huang Xinjing received the B.Sc. and Ph.D. degrees in instrument science and technology from Tianjin University, Tianjin, China, in 2010 and 2016, respectively.

In 2016, he joined the Modern Acoustic Testing Laboratory of Tianjin University as an Assistant Professor. Since 2020, he has been an Associate Professor at the School of Precision Instrument and Opto-Electronics Engineering, Tianjin University. He also works at the State Key Laboratory of Precision Measurement Technology and Instruments, Tianjin University. His research topics mainly cover structural health inspection and/or monitoring technology, acoustic metamaterial device and sensor, magnetic/acoustic sensing and measurement, and intelligent perception electronic system.

Ren Xiaoyu received the B.E. degree from Chongqing University, Chongqing, China, in 2022. He is currently pursuing the master's degree with the Instrument Science and Technology Department, Tianjin University, Tianjin, China.

His research interests include acoustic sensors and metamaterials.

Wang Liang, photograph and biography not available at the time of publication.

Bian Xu received the Ph.D. degree from Tianjin University, Tianjin, China, in 2016.

He is currently a postdoctoral researcher with the Instrument Science and Technology Department, Tianjin University, and a Lecturer at Tianjin Renai College, Tianjin. His research interests include pressure vessel leakage detection and structural health monitoring.

Li Jian received the B.E., M.E., and Ph.D. degrees from Tianjin University, Tianjin, China, in 1994, 1997, and 2000, respectively.

He is currently a Professor with Tianjin University. His research interests include pipeline leak detection and pipeline safety warning.

Ma Jinyu received the B.E. and M.E. degrees in instrument science and technology from Shandong University of Science and Technology, Qingdao, China, in 2010 and 2012, respectively, and the Ph.D. degree in instrument science and technology from Tianjin University, Tianjin, China, in 2016.

In 2016, she joined as a Lecturer and Engineer at the Sensor and Electronic Testing Laboratory, Tianjin University, where she is also with the State Key Laboratory of Precision Measurement Technology and Instruments. Her main research interests include acoustic and electric sensing and measurement systems.